PSR-Based Microstructural Modeling for Turbulent Combustion Processes and Pollutant Formation in Double Swirler Combustors

Seong-Ku Kim, Sung-Mo Kang, Yong-Mo Kim*
Department of Mechanical Engineering, Hanyang University
Jeong-Lak Sohn
School of Mechanical and Aerospace Engineering, Seoul National University

The present study numerically investigates the fuel-air mixing characteristics, flame structure, and pollutant emission inside a double-swirler combustor. A PSR (Perfectly Stirred Reactor) based microstructural model is employed to account for the effects of finite rate chemistry on the flame structure and NO formation. The turbulent combustion model is extended to nonadiabatic flame condition with radiation by introducing an enthalpy variable, and the radiative heat loss is calculated by a local, geometry-independent model. The effects of turbulent fluctuation are taken into account by the joint assumed PDFs. Numerical model is based on the non-orthogonal body-fitted coordinate system and the pressure/velocity coupling is handled by PISO algorithm in context with the finite volume formulation. The present PSR-based turbulent combustion model has been applied to analyze the highly intense turbulent nonpremixed flame field in the double swirler combustor. The detailed discussions were made for the flow structure, combustion effects on flow structure, flame structure, and emission characteristics in the highly intense turbulent swirling flame of the double swirler burner.

Key Words : PSR-Based Microstructural Model, Turbulent Nonpremixed Flames, NOx Emission, Double Swirler Combustors

Nomenclature

$a_{P,k}$: Absorption coefficient of kth species
CO : Carbon Monoxide
e : Enthalpy variable (dimensionless)
f : Mixture fraction
g : Variance of mixture fraction
h : Total static enthalpy
NO_x : Nitrogen Oxides
P : Probability density function
Q_{rad} : Radiative heat loss rate per unit volume
U : Difference between adiabatic and minimum enthalpy at a given mixture fraction
U_{ff} : Second derivative of U
χ : Scalar dissipation rate
δ : Dirac delta function
σ_B : Stefan-Boltzmann constant
τ : Residence time of local PSRs

Superscript

$\sim$: Favre (density-weighted) averaging

* Corresponding Author,
E-mail : ymkim@email.hanyang.ac.kr
TEL : +82-2-2290-0428 ; **FAX** : +82-2-2297-0339
Department of Mechanical Engineering, Hanyang University, San 17, Hangdang-dong, Sungdong-gu, Seoul 133-791, Korea. (Manuscript **Received** February 17, 2000; **Revised** September 18, 2000)

1. Introduction

The strict emission regulation has become a major technology driver for the gas turbine industry. NOx, CO, and unburned hydrocarbons are regulated from base load down to varying degrees of part load. In order to achieve the low NOx emission, the combustor designers have only the limited options including catalytic combustion, lean direct injection of fuel, premixed combustion and rich-quench-lean combustion.

Through a series of consistent experimental

studies (Hayashi et al. 1998 ; Terasaki and Hayashi., 1996), Hayashi et al. have demonstrated the capability of low-NOx emissions of nonpremixed lean direct fuel injection burners which are completely free from the serious drawbacks of lean premixed combustor such as autoignition, flashback and combustion instability. These burners take advantages of the strong mixing of fuel and excess combustion air by strongly swirling flows or interacting impingement of fuel jets, and achieve the low-NOx emissions over the wide range of inlet air temperature, while maintaining high combustion efficiency even near flame stability limit. Instead of premixing fuel and air upstream the combustion region, rapid mixing of fuel, excessive air, and burned gas is used not only to suppress the formation of fuel-rich gas pockets but also to shorten the life time of hot gas pockets which are the major source for NOx formation.

The present study has been motivated to develop the turbulent combustion model which is capable of predicting the detailed flame structure and the pollutant emission of the lean direct fuel injection burners with the computationally efficient and physically realistic ways. A number of numerical approaches are now potentially capable of simulating the turbulent reacting flows. These approaches include flamelet models (Ferreira, 1996), reaction progress variable (RPV) models (Louis, 1997 ; Kim et al., 2000), conditional moment closure (CMC) (Klimenko et al., 1999 ; Kim et al., 2000), PEUL model (Schlatter, 1997) and PDF transport model (Correa, 1996). These methods coupled with reduced and detailed chemistry have been emerged as the promising tools for simulating the turbulent reacting flows. Reduced chemistry schemes are often used in the turbulent combustion modeling, with success on certain issues and/or over limited sets of conditions. However, the full chemistry schemes are often needed to analyze the higher order hydrocarbon chemistry, the soot formation and oxidation processes, and so on. The laminar flamelet model offers one of the convenient ways to incorporate the detailed chemistry. However, in order to analyze the highly intense turbulent flame field in the lean direct fuel injection combustors, the turbulent combustion models must have the capabilities to handle the distributed reaction zones with the thickened flame. In the distributed reaction regimes, the turbulent mixing time scales are comparable to the chemical reaction time scales, i. e., the Damkohler number of many of the reactions is of order of unity or less. The laminar flamelet model is not applicable to these thickened flame fields. Hu and Correa (1996) developed the PSR microstructual model which brings the complex chemistry to bear within the distributed reaction zone regime, at the relatively low computational cost of the assumed shape PDF/k-ε-g model. In their PSR-based combustion model, the microstructure of the distributed

The present PSR-based turbulent combustion model has been applied to analyze the highly intense turbulent nonpremixed flame field in the double swirler combustor (DSC). Computations are carried out for the nonreacting and reacting turbulent swirling flows of DSC. Based on numerical results, the detailed discussions were made for the flow structure, combustion effects on flow structure, flame structure, and emission characteristics in the highly intense turbulent swirling flame of the double swirler burner.

2. Physical and Numerical Modeling

2.1 PSR-based microstructural model

In a nonpremixed turbulent flame, the thermochemical properties can be characterized by the mixture fraction and the residence time. In intensely turbulent flames, the residence time could be quantified using scalar dissipation rate. The lower dissipation rate corresponds to the longer time for reactions (i. e., the large microscale residence time). Thus turbulent flame properties can be described by the PDFs of mixture fraction and scalar dissipation rate (or microscale residence time). The turbulent eddy structure of the distributed reaction zone is modeled as a distribution of PSRs over a range of mixture fractions and residence times. Therefore, the instantaneous thermochemical state of a mixture in a nonpremixed adiabatic flame condition can

now be determined by mixture fraction, f and residence time, τ. Prior to a flame calculation, all the thermochemical properties such as temperature, species concentrations, density are calculated by using a PSR code over the allowable range of mixture fractions and residence times.

The density-weighted (Favre-averaged) properties of the reacting mixture are evaluated by convoluting the instantaneous properties with the joint probability distribution:

$$\tilde{\phi}=\int_0^\infty\int_o^1 \phi(f,\ \tau)\cdot\tilde{P}(f,\ \tau)dfd\tau \tag{1}$$

Here, mixture fraction and residence time are assumed to be statistically independent, so that the assumed joint probability density function can be constructed as

$$\tilde{P}(f,\ \tau)=\tilde{P}_1(f)*\tilde{P}_2(\tau) \tag{2}$$

The PDF for residence time, $P_2(\tau)$ can be obtained from a relationship between residence time and scalar dissipation rate as follows, according to Hu and Correas suggestion (Hu et al., 1996).

The residence time, τ in a turbulent eddy PSR is

$$\tau=C\frac{\tilde{g}}{\chi} \tag{3}$$

Based on Eq. (3), $P_2(\tau)$ can be obtained from the pdf of scalar dissipation $P_3(\chi)$ as

$$\tilde{P}_2(\tau)=\frac{\chi^2}{C\tilde{g}}\tilde{P}_3(\chi) \tag{4}$$

Here, $P_3(\chi)$ is taken to be log-normal function (Lentini, 1994).

$$\tilde{P}_3(\chi)=\frac{1}{\chi\sigma\sqrt{2\pi}}\exp\left[-\frac{(\ln\chi-\mu)^2}{2\sigma^2}\right] \tag{5}$$

where, μ is the mean and σ is the standard deviation of $\ln\chi$, and are related to the mean scalar dissipation rate and local turbulent Reynolds number as

$$\tilde{\chi}=\exp\left[\mu+\frac{\sigma^2}{2}\right] \text{ and } \sigma^2=\frac{1}{2}\frac{\ln\sqrt{Re}}{10} \tag{6}$$

The mean scalar dissipation rate is related to the local turbulent kinetic energy, the local dissipation rate, and the local variance of mixture fraction, as follows

$$\tilde{\chi}=C_{g2}\frac{\tilde{\varepsilon}}{\tilde{k}}\tilde{g} \tag{7}$$

Therefore, as a consequence, Eq. (1) can be expressed as

$$\begin{aligned}\tilde{\phi}&=\int_{\tau_{ex}}^\infty\int_o^1\phi(f,\ \tau)\cdot\tilde{P}(f,\ \tau)dfd\tau\\&\quad+\int_0^{\tau_{ex}}\int_o^1\phi(f,\ \tau)\cdot\tilde{P}(f,\ \tau)dfd\tau\\&=\sum_{l=2}^{L}\phi^*(\tau_l)\int_{\tau_{l-1/2}}^{\tau_{l+1/2}}\tilde{P}_2(\tau)d\tau\\&\quad+\phi^*(\tau_1)\int_0^{\tau_{ex}}\tilde{P}_2(\tau)d\tau\end{aligned} \tag{8}$$

where

$$\phi^*(\tau_l)=\int_0^1\phi(f,\ \tau_l)\cdot\tilde{P}_1(f)df \tag{9}$$

The integral shown in Eq. (8) can be expressed in terms of error function as follows

$$\int_{\tau_{l-1/2}}^{\tau_{l+1/2}}\tilde{P}_2(\tau)d\tau=\frac{1}{2}[erf(\theta_{l+1/2})-erf(\theta_{l-1/2})] \tag{10}$$

where

$$\theta_l=\frac{\ln\tau_l-\mu_\tau}{\sqrt{2}\sigma} \text{ and } \mu_\tau=\ln\left(\frac{C\tilde{k}}{C_{g2}\tilde{\varepsilon}}\right)+\frac{\sigma^2}{2} \tag{11}$$

2.2 PDF of mixture fraction

The beta function has been most widely used for assumed PDF of mixture fraction. However, It is slower to get the mean scalar quantities by integration, and it may sometimes lead to singularity difficulties in numerical simulation. The clipped-Gaussian function also gives reasonable results, but it is very time-consuming to determine the model parameters due to solving a set of non-linear equations for each integration. Zhou et al. (1997) proposed a multi-delta function, which has the advantage of both the simplicity of the double-delta model and the reasonability of the clipped-Gaussian model.

Multi-delta PDF:

$$\tilde{P}_1(f)=\sum_{i=-n}^{n}P_n(i)\cdot\delta(f_i) \tag{12}$$

where

$$f_i=\tilde{f}+i\sqrt{\frac{\tilde{g}}{\sum_{k=-n}^{n}k^2P_n(k)}} \tag{12a}$$

and

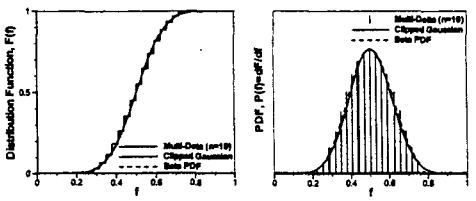

(a) f=0.5, g=0.0125

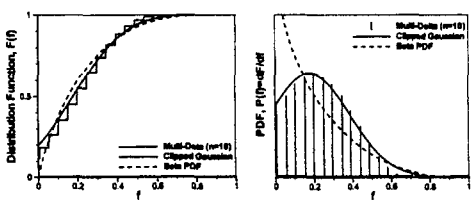

(b) f=0.2 and g=0.03

Fig. 1 Distribution functions and probability density functions of multi-delta, clipped Gaussian, and beta PDF models

$$P_n(i)=\frac{\sin^2\left[\frac{\pi(n-|i|)}{2n}\right]}{\sum_{k=-n}^{n}\sin^2\left[\frac{\pi(n-|k|)}{2n}\right]} \tag{12b}$$

Figure 1 presents comparison of distribution functions and its derivatives, i. e., probability density functions. The predicted results with the three PDF models for mixture fraction have demonstrated, though not presented here, that the preditive capabilities of clipped Gaussian and multi-data PDF models are almost identical, but that there are some difference compared to that of beta PDF, especially near lean or rich mixtures, as would be expected in Fig. 1.

2.3 Extension to non-adiabatic flame

When the radiative heat loss is taken into account, enthalpy transport is no longer described by the mixture fraction transport equation. Thus, in numerically modeling the non-adiabatic flame field, a transport for a separate enthalpy variable must be solved. A normalized enthalpy is utilized for improving statistical independence from the mixture fraction as well as for convenience in governing lookup table (Kim et al., 2000):

$$e=\frac{h-h_{\min}}{h_{ad}-h_{\min}}=\frac{h-h_{\min}}{U(f)} \tag{13}$$

Here, h and h_{ad} are the total static enthalpy and the adiabatic enthalpy, respectively. The minimum enthalpy, h_{min} is defined as the enthalpy of the mixture in equilibrium state at temperature corresponding to the inert mixing.

The present study assumes that the flame is optically thin so that radiation source term can be determined locally only by emission. This optically thin radiation model allows the computationally manageable procedure for the turbulent flame calculations because the radiation source term must be computed prior to flame calculation to consider the effect of turbulent fluctuation via the probability density functions.

With the assumption of the optically thin limit, the radiative loss rate per unit volume can be expressed as

$$Q_{rad}(T,\ Y_k)=4\sigma_B\sum(P_k\cdot a_{P,k})(T^4-T_b^4) \tag{14}$$

Here, four species H_2O, CO_2, CO, and CH_4 are taken to participate in radiation and more detailed informations can be found in the web site of TNF workshop (TNF workshop web site).

The transport equation of mean enthalpy variable is derived as follows

$$\frac{\partial}{\partial t}(\bar{\rho}\tilde{e})+\frac{\partial}{\partial x_j}(\bar{\rho}\tilde{u}_j\tilde{e})=\frac{\partial}{\partial x_j}\left(\frac{\mu_{eff}}{\sigma_e}\frac{\partial\tilde{e}}{\partial x_j}\right)+(\tilde{e}-1)C_g\frac{\overline{U_{ff}}}{U}\bar{\rho}\tilde{g}\frac{\tilde{\varepsilon}}{\tilde{k}}-\frac{\overline{Q_{rad}}}{U} \tag{15}$$

In the present study, the single-delta PDF is used for enthalpy variable as the shape of PDF for enthalpy variable has the negligibly small influence on the result (Louis, 1997).

2.4 Numerical model

The governing equations on the non-orthogonal body-fitted coordinate system are discretized by the finite volume method with a TVD type high-order upwind scheme for convection terms and the central differencing scheme for diffusion terms. Non-staggered grid arrangement is used and PWIM (pressure weighted interpolation method) is adopted to prevent a pressure oscillation. Pressure-velocity coupling is handled by PISO algorithm. To improve convergence in highly swirling flow calculations, the centrifugal force term appearing in the radial momentum equation is implicitly treated by utilizing the

discretized tangential momentum equation (Jang et al., 1998). More detailed information can be found elsewhere (Kim et al., 1994).

3. Results and Discussion

To evaluate the predicative capability of the present PSR-based turbulent combustion model. The highly intense turbulent swirling flame in the double swirler combustor (Terasaki et al., 1996) have been chosen. Figure 2 shows the schematic configuration of the double swirler combustor and the main components including an upstream swirler set and a flame tube of 300 mm in length and 80 mm in diameter. The swirler set consists of coaxial and corotational swirlers with 16 curved vanes of an angle of 45°. Combustion air is influxed through inner circular and outer annular passages with a ratio of about 1:2. Air entering through the inner passage mixes with gaseous fuel injected from multi-hole nozzle at angle of 60° and the combustible mixture is substantially accelerated by passing through the converging duct, which is designed to prevent flashback ,and autoignition. Computations are performed for two experimental conditions listed below. Here, methane is used as fuel and the reference air velocity, U_{ref} denotes the mean velocity of air averaged over the cross sectional area of flame tube.

As shown in Fig. 2, the grid arrangement is based on the 210×54 nonuniform grid. The computational domain extends up to $x=0.4$m for ensuring the numerical convergence especially in the reacting flow calculations. In order to avoid the excessive computing time in the 3D simulations, the double swirler combustor is axisymmetrically modeled by modifying the fuel nozzle to an annular injector at the given fuel mass flow rate. At the inlet boundaries with the swirler vanes, the axial and tangential velocities are uniformly imposed according to the given flow rate and the vane swirl angle.

In order to understand the basic flow structure of the double swirler combustor, the nonreacting turbulent swirling flows are initially analyzed. Figure 3 shows the predicted velocity vectors for the double swirler combustor and the conventional burner with a large hub swirler (Terasaki et al. 1996). Strong swirling flows in the two burners are characterized with the existence of a large central toroidal recirculation zone (CTRZ) and an accompanying corner recirculation zone. However, there are the distinct differences in the detailed flow structures and mixing patterns of two swirl combustors.

Compared to the conventional swirler, the double swirler creates the much stronger and wider CTRZ with its apex up to the throat and the resulting air/fuel mixing process is greatly enhanced due to opposing effect of the reversed flow and the high-velocity jet issued through the converging duct. For the conventional burner, the large portion of fuel jet penetrates the upstream recirculation zone and they mix with the annular air jet. Consequently, the conventional swirler yields the much slower air/fuel mixing process which leads to the formation of locally fuel-rich

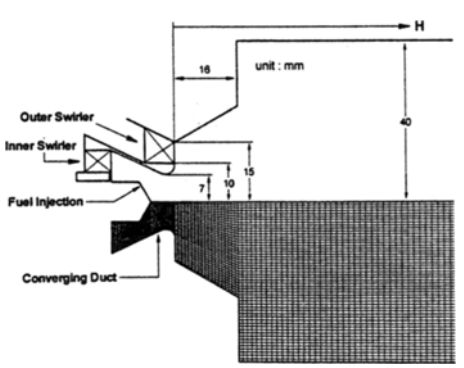

Fig. 2 Schematics and grid system for a double swirler combustor

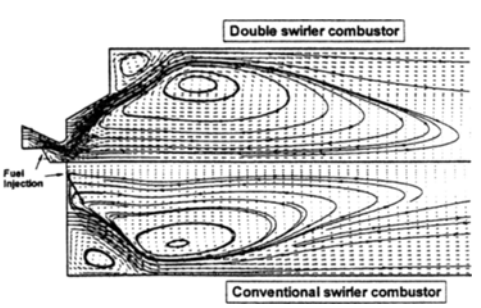

Fig. 3 Predicted velocity vectors and streamlines for the double swirler combustor and the conventional burner under the nonreacting condition

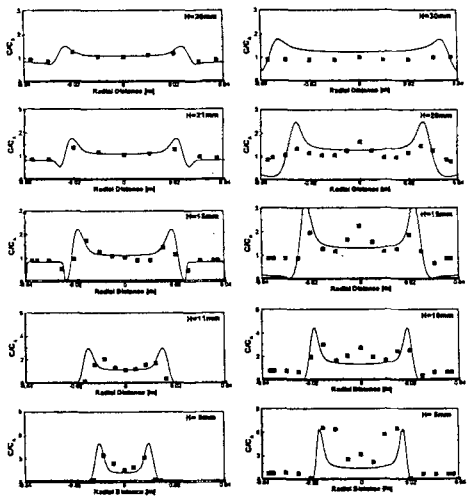

Fig. 4 Distribution of normalized fuel concentration within the double swirler combustor (left) and the conventional swirl combustor (right) under the nonreacting condition

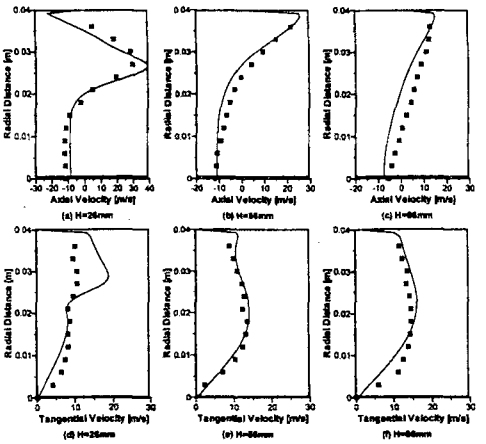

Fig. 5 Radial profiles of axial and tangential velocities for the double swirler combustor under the nonreacting condition

regions especially in the upstream locations. The radial profiles of normalized fuel concentration shown in Fig. 4 clearly indicate these mixing trend. The double swirler forms the highly uniform mixtures in a very short distance from the injector. This enhanced aerodynamically -controlled mixing process between fuel jet and swirling air jet is very effective in suppressing NOx formation when the combustion takes place.

To evaluate the predicative capability of the standard k-ε model in the swirling flows, the predicted and measured radial profiles of axial and tangential velocities in the double swirler combustor are presented in Fig. 5. In terms of the strength and location of the centerline reversal velocity, the standard k-ε model favorably agrees with experimental data. However, there are the quantitative differences between prediction and measurement. Figure 5(d) and 5(f) indicate the present procedure yields the overestimation of the angular momentum flux and the rapid decay of tangential velocity to a solid-body rotation downstream. These discrepancies are mainly attributed to the defect of standard k-ε model based on the isotropic viscosity assumption and the uncertainties in swirler exit boundary conditions.

In the next stage, the present PSR-based microstructual combustion model has been applied to predict the turbulent reacting flows in the double swirler combustor. In this study, the PSR-based library was constructed over the allowable range of mixture fractions, residence times, and enthalpy variables by using the full GRI 2.11 mechanism for methane-air combustion, which contains 277 elementary chemical reactions of 49 species including nitrogen chemistry (Bowman et al., GRI-Mech 2.11). Figure 6 presents a data base of temperature and mass fraction of CO and NO in the f-τ plane at the adiabatic (e= 1.0) and nonadiabatic (e=0.85) condition. The maximum peaks of temperature occur along the stoichiometry (f_{st}=0.055) and the temperature is decreased by reducing the residence time. When residence time decreases below a certain value, the PSR reaches to the flame-out condition unable to sustain combustion and then its outlet temperature drops suddenly to inlet temperature. With approaching to this flame-out condition, CO concentration increases due to the increase of the incomplete combustion. The NO concentration has its maximum values at the slightly lean side of stoichiometry and it almost linearly increases by increasing the residence time. By increasing the deviation from adiabatic flame condition, the temperature, and the concentration of CO and NO decrease owing to the increased radiative heat loss.

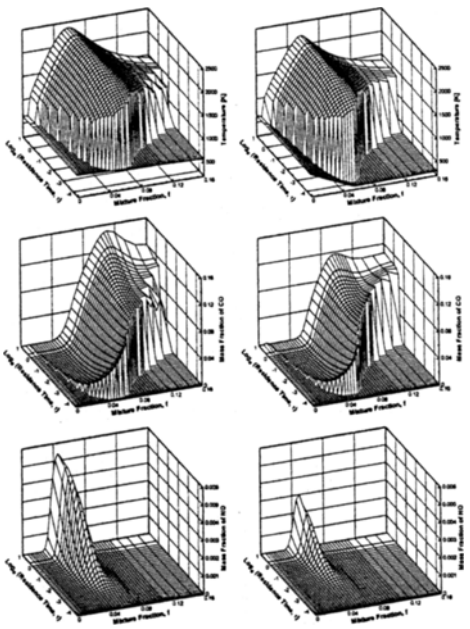

Fig. 6 PSR-based library presented in the f-τ plane at the adiabatic (e=1) and nonadiabatic (e =0.85) conditions for a methane-air flame (T_{in}=650K, f_{st}=0.055)

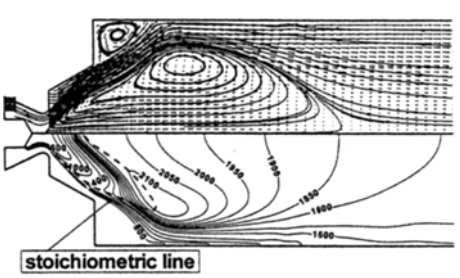

Fig. 7 Predicted velocity vectors and temperature contours for the double swirler combustor under the burning condition

Figure 7 shows the predicted velocity vectors and the temperature fields for the double swirler combustor. The combustion processes significantly modify the swirling flow structure in terms of length, width, and strength of CTRZ. This is mainly caused by the gas expansion effects which include the thickness increase in the shear layer of recirculation zone, an early closure of the recirculation zone, and the decrease in length of CTRZ. However, it is necessary to note that the k-ε turbulence model exaggerate this tendency.

In order to check the validity of the present

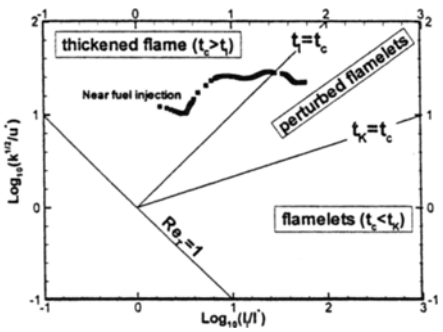

Fig. 8 The turbulent combustion regime of the double swirler combustor (modified Borghi's diagram)

PSR-based microstructual combustion model in this highly intense turbulent reacting flow, based on the reference scales of time, length, and velocity for nonpremixed flames, the modified Borghis diagram of combustion regimes (Lentini, 1994) are plotted in Fig. 8. Along the reaction front in the turbulent flames of DSC, the combustion processes mostly occur at the distributed reaction regime. This result confirms that the present PSR-based microstructual combustion model is valid for the combustion regime of DSC.

Figures 9 and 10 show the predicted and measured radial profiles of temperature and equivalence ratio at several axial stations. Numerical results are obtained by three combustion models including the equilibirum model, the PSR-based model, and the PSR-based model accounting for radiative heat loss. Near the exit of double swirler, three combustion models predict significant temperature peaks, which was not captured in measurement (Terasaki et al., 1996). These qualitative differences are directly tied with the incorrect peaks of mean mixture fraction shown in Fig. 10. This discrepancy is mainly due to the rough modeling of the 3-D fuel injection process. In the downstream locations (H> 35mm), all models predict the qualitatively correct trend. In prediction of temperature and equivalence ratio at the primary combustion zone, the PSR-based model yields the improved results over the equilibrium model. However, in the upstream corner recirculation zone, the PSR-based models considerably underpredict the tem-

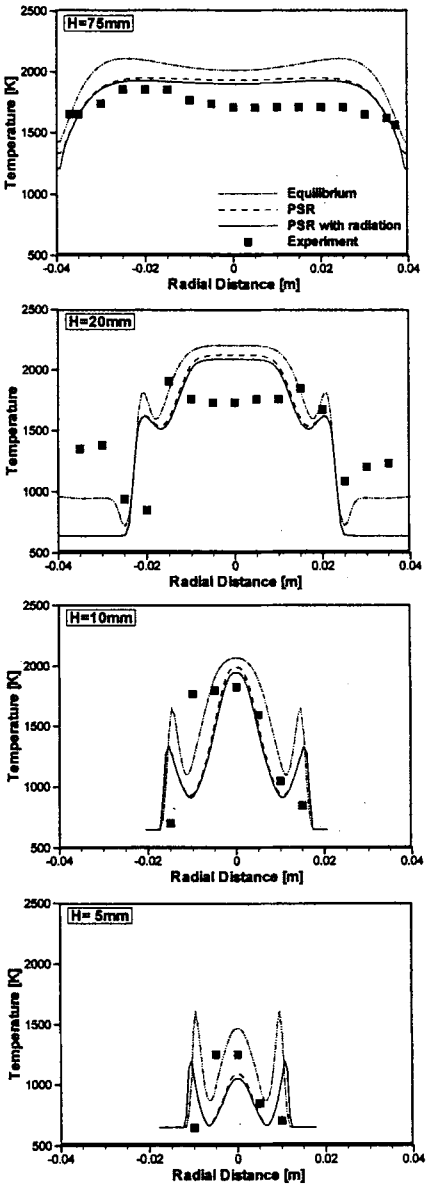

Fig. 9 Radial profiles of temperature within the double swirler combustor

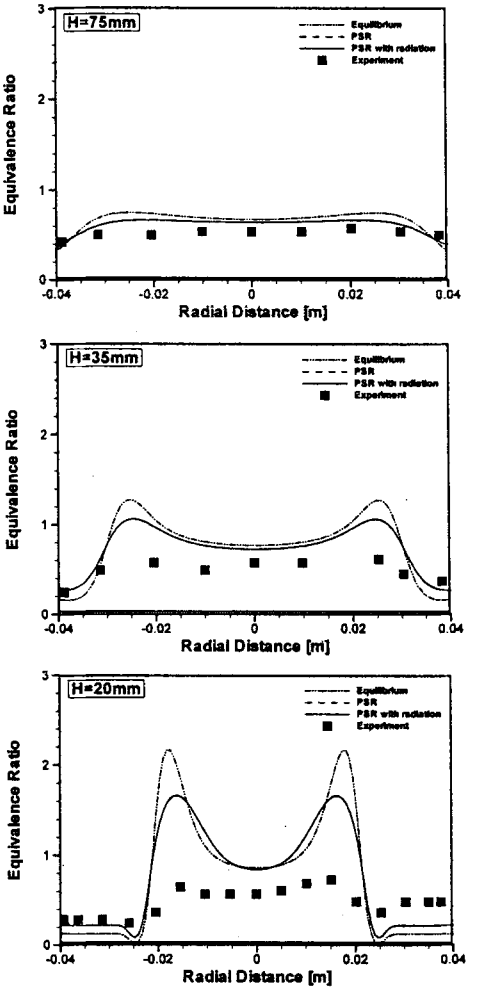

Fig. 10 Radial profiles of local equivalence ratio within the double swirler combustor

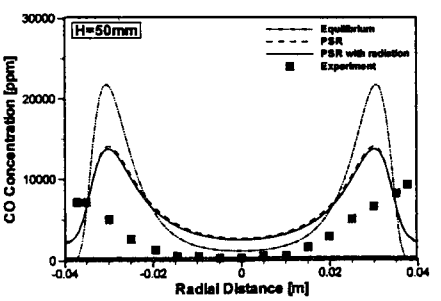

Fig. 11 Radial profiles of CO concentration within the double swirler combustor

perature distribution which is nearly to the inert state. This might be caused by the defect of the PSR-based model, which leads to substantially underpredict the reactedness for lean or rich mixture. Numerical results also indicate that the effect of radiative heat loss on temperature distribution is marginally important for this highly intense turbulent flame.

Figure 11 shows the predicted and measured radial profile of CO concentration at H=50mm. Compared to the equilibrium model, the PSR-based models made the noticeable improvement

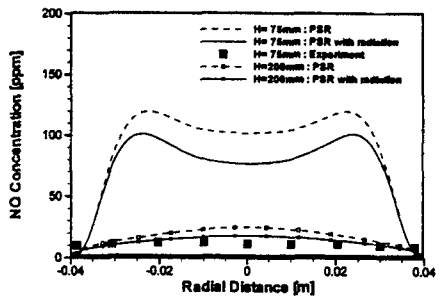

Fig. 12 Radial profiles of NO concentration within the double swirler combustor

for predicting the peak level of CO concentration. The radial profiles of NO concentration at H= 75mm and 200mm are presented in Fig. 12. At the relatively upstream location (H=75 mm), two PSR-based models considerably overestimate the NO concentration. The overprediction of NO in the recirculation zone is attributed mainly to the overestimation of flame temperature. But, at the far downstream location (H=200 mm), the predicted NO level is quite close to the experimental data. It is also found that the effect of the radiative heat loss on the NO formation is quite noticeable in this DSC flame field.

4. Conclusions

The present PSR-based turbulent combustion model has been applied to analyze the highly intense turbulent nonpremixed flame field in the double swirler combustor. Based the computational results, the following conclusions can be drawn:

(1) Compared to the conventional swirler, the double swirler creates the much stronger and wider CTRZ with its apex up to the throat and the resulting air/fuel mixing process is greatly enhanced due to opposing effect of the reversed flow and the high-velocity jet issued through the converging duct.

(2) The combustion processes significantly modify the swirling flow structure in terms of length, width, and strength of CTRZ. This is mainly caused by the gas expansion effects which include the thickness increase in the shear layer of recirculation zone, an early closure of the recirculation zone, and the decrease in length of CTRZ.

(3) Compared to the equilibrium model, the PSR-based models made the noticeable improvement for predicting the peak level of CO concentration. At the relatively upstream location(H= 75mm), two PSR-based models considerably overestimate the NO concentration. But, at the far downstream location (H=200mm), the predicted NO level is quite close to the experimental data. It is also found that the effect of the radiative heat loss on the NO formation is quite noticeable in this DSC flame field.

(4) The present PSR-based microstructural combustion model together with the joint PDF model and the geometry-independent radiation model successfully predict the main features of the highly intense turbulent reacting flows in the double swirler combustor. However, there exist the considerable deviations between prediction and measurement. These discrepancies are mainly attributed to the defect of turbulence model and combustion model, uncertainties in the swirler exit boundary conditions, and experimental errors.

(5) The future work includes the critical validation of the present PSR-based turbulent combustion model against the detailed experimental data based on the reliable combustion diagnostics.

References

Bowman, C. T., Hanson, R. K., Davidson, D. F., Gardiner, Jr., W. C., Lissianski, V., Smith, G. P., Golden, D. M., Frenklach, M., and Goldenberg, M., GRI-Mech 2. 11, http://www. me. berkeley. edu/gri_mech/.

Correa, S. M., Hu, I. Z., and Tolpadi, A. K., 1996, Combustion Technology for Low-Emissions Gas Turbines : Some Recent Modeling Results, *J. Energy Resources Technology*, Vol. 118, pp. 201~208.

Ferreira, J. C., 1996, Flamelet Modelling of Stabilization in Turbulent Non-premixed Combustion, PhD Thesis, ETHZ Zuerich Switzerland.

Hayashi, S., Yamada, H., Shimodaira, K, and

Machida, T, 1998, NOx Emissions from Non-premixed, Direct Fuel Injection Methane Burners at High-Temperature and Elevated Pressure Conditions, *27th Symp. (Int.) on Combustion*, The Combustion Institute, pp. 1833~1839.

Hu, I. Z. and Correa, S. M., 1996, Calculations of Turbulent Flames Using a PSR Microstructural Library, *26th Symp. (Int.) on Combustion*, The Combustion Institute, pp. 307~313.

Jang, D. S. and Acharya, S., 1988, Source Decomposition to Improve Convergence of Swirling Flow Calculations, *AIAA J.*, Vol. 26, No. 3, pp. 372~374.

Kim, S. H., Huh, K. Y., and Tao, L., 2000, Application of the Elliptic Conditional Moment Closure Model to a Two-Dimensional Non-premixed Methanol Bluff-Body Flame, *Combustion and Flame*, Vol. 120, pp. 75~90.

Kim, S. K., Kim, Y. M., Ahn, K. Y. and Oh, K., 2000, Numerical Modeling for the H_2/CO Bluff-Body Stabilized Flames, *KSME International Journal*, Vol. 14, No. 8, pp. 879~890.

Kim, Y. M., Shang, H. M., Chen, C. P., and Wang, T. S., 1994, Prediction of Confined Swirling Spray-Combusting Flows, *Numerical Heat Transfer*, Part A, Vol. 25, pp. 1~19.

Klimenko, A. Y. and Bilger, R. W., 1999, Conditional Moment Closure for Turbulent Combustion, *Prog. in Energy and Combust. Sci.*, Vol. 25, pp. 595~687.

Lentini, D., 1994, Assessment of The Stretched Laminar Flamelet Approach for Nonpremixed Turbulent Combustion, *Combust. Sci. and Tech.*, Vol. 100, pp. 95~122.

Louis, J. J. J., 1997, On Turbulent Combustion of Coal Gas, Ph. D Thesis, Univ. of Twente, Enschede.

Schlatter, M., 1997, Modelling of Turbulence-Chemistry Interactions with Respect to the NOx Formation in Turbulent Non-premixed Flames, PhD Thesis, ETHZ Zuerich Switzerland.

Terasaki, T. and Hayashi, S., 1996, The Effects of Fuel-Air Mixing on NOx Formation in Non-Premixed Swirl Burners, *26th Symp. (Int.) on Combustion*, The Combustion Institute, pp. 2733~2739.

TNF workshop web site, http://www. ca. sandia. gov/tdf/Submodels. htm.

Zhou, L., Zhang, H., and Lin, W., 1997, A Multi-δ-PDF Model of Turbulent Combustion, 1_{st} *Asia-Pacific Conference on Combustion*, pp. 194~197.